AGU PUBLICATIONS

Geophysical Research Letters

RESEARCH LETTER
10.1002/2016GL069166

Special Section:
First results from NASA's Magnetospheric Multiscale (MMS) Mission

MMS observations of large guide field symmetric reconnection between colliding reconnection jets at the center of a magnetic flux rope at the magnetopause

M. Øieroset[1], T. D. Phan[1], C. Haggerty[2], M. A. Shay[2], J. P. Eastwood[3], D. J. Gershman[4,5], J. F. Drake[6], M. Fujimoto[7], R. E. Ergun[8], F. S. Mozer[1], M. Oka[1], R. B. Torbert[9,10], J. L. Burch[10], S. Wang[4,5], L. J. Chen[4,5], M. Swisdak[11], C. Pollock[12], J. C. Dorelli[4], S. A. Fuselier[10,13], B. Lavraud[14,15], B. L. Giles[4], T. E. Moore[4], Y. Saito[7], L. A. Avanov[4,5], W. Paterson[4], R. J. Strangeway[16], C. T. Russell[16], Y. Khotyaintsev[17], P. A. Lindqvist[18], and K. Malakit[19]

[1]Space Sciences Laboratory, University of California, Berkeley, California, USA, [2]Department of Physics and Astronomy, University of Delaware, Newark, Delaware, USA, [3]The Blackett Laboratory, Imperial College London, London, UK, [4]NASA Goddard Space Flight Center, Greenbelt, Maryland, USA, [5]Department of Astronomy, University of Maryland, College Park, Maryland, USA, [6]Department of Physics and the Institute for Physical Science and Technology, University of Maryland, College Park, Maryland, USA, [7]ISAS/JAXA, Sagamihara, Japan, [8]LASP, University of Colorado Boulder, Boulder, Colorado, USA, [9]Institute for the Study of Earth, Oceans, and Space, University of New Hampshire, Durnham, New Hampshire, USA, [10]Southwest Research Institute, San Antonio, Texas, USA, [11]Institute for Research in Electronics and Applied Physics, University of Maryland, College Park, Maryland, USA, [12]Denali Scientific, Healy, Alaska, USA, [13]Department of Physics and Astronomy, University of Texas at San Antonio, San Antonio, Texas, USA, [14]Institut de Recherche en Astrophysique et Planétologie, Université de Toulouse, Toulouse, France, [15]Centre National de la Recherche Scientifique, Toulouse, France, [16]Department of Earth, Planetary, and Space Sciences, University of California, Los Angeles, California, USA, [17]Swedish Institute of Space Physics, Uppsala, Sweden, [18]Royal Institute of Technology, Stockholm, Sweden, [19]Department of Physics, Mahidol University, Bangkok, Thailand

Key Points:
- First report of magnetic reconnection in a compressed thin current sheet between colliding jets at the center of a magnetic flux rope
- Large guide field causes asymmetries in plasma and field structures in the reconnection layer
- Excellent agreement in plasma and field profiles between observations and 2-D particle-in-cell simulation

Correspondence to:
M. Øieroset,
oieroset@ssl.berkeley.edu

Citation:
Øieroset, M., et al. (2016), MMS observations of large guide field symmetric reconnection between colliding reconnection jets at the center of a magnetic flux rope at the magnetopause, *Geophys. Res. Lett.*, *43*, 5536–5544, doi:10.1002/2016GL069166.

Received 14 APR 2016
Accepted 9 MAY 2016
Accepted article online 12 MAY 2016
Published online 4 JUN 2016

Abstract We report evidence for reconnection between colliding reconnection jets in a compressed current sheet at the center of a magnetic flux rope at Earth's magnetopause. The reconnection involved nearly symmetric inflow boundary conditions with a strong guide field of two. The thin (2.5 ion-skin depth (d_i) width) current sheet (at ~12 d_i downstream of the X line) was well resolved by MMS, which revealed large asymmetries in plasma and field structures in the exhaust. Ion perpendicular heating, electron parallel heating, and density compression occurred on one side of the exhaust, while ion parallel heating and density depression were shifted to the other side. The normal electric field and double out-of-plane (bifurcated) currents spanned almost the entire exhaust. These observations are in good agreement with a kinetic simulation for similar boundary conditions, demonstrating in new detail that the structure of large guide field symmetric reconnection is distinctly different from antiparallel reconnection.

1. Introduction

Collisionless magnetic reconnection is a universal plasma process that converts magnetic energy to particle energy. The process is initiated at an X line in a thin current sheet and can occur for both asymmetric and symmetric density and magnetic field boundary conditions, and for a wide range of magnetic shear/guide field.

The studies of processes near the X line in the strong guide field regime have been explored in numerous simulation studies, where it has been found that the strong guide field affect the current system significantly and leads to strong asymmetries in both the plasma and field profiles across the reconnection layer [e.g., *Pritchett and Coroniti*, 2004; *Drake and Swisdak*, 2014].

The strong guide field regime near the X line is much less explored observationally due to the rarity of such observations in near-Earth space. Reconnection at the magnetopause tends to involve highly asymmetric inflow plasma conditions, while magnetotail reconnection typically involves symmetric inflow conditions but with a small guide field [*Eastwood et al.*, 2010a, 2010b]. Observations in the magnetotail revealed that even a small guide field can give rise to asymmetries in the plasma and field profiles across the exhaust [*Eastwood et al.*, 2010b; *Wang et al.*, 2012].

Symmetric reconnection with a variety of guide fields often occurs in solar wind current sheets [e.g., *Gosling et al.*, 2005; *Gosling and Szabo*, 2008; *Phan et al.*, 2010; *Gosling and Phan*, 2013], but the observations are usually far downstream of the X line. In recent years, symmetric reconnection has also been reported in current sheets in the magnetosheath [e.g., *Retino et al.*, 2007; *Phan et al.*, 2007a, 2007b, 2011], but some of these thin current sheets were not resolved by past plasma measurements.

Here we report Magnetospheric Multiscale (MMS) observations of a well-resolved symmetric reconnection layer in the presence of a strong guide field in yet another type of phenomenon. The reconnection event occurred in a thin current sheet between two colliding jets in a flux rope at the magnetopause. Thin current sheets inside flux ropes flanked by active X lines have previously been reported but were not resolved by previous plasma instrumentation [*Hasegawa et al.*, 2010; *Øieroset et al.*, 2011, 2014]. In the event reported here MMS crossed a large-scale magnetopause flux rope (~100 d_i diameter) and observed a thin (2.5 d_i) reconnecting current sheet at the flux rope center. The current sheet crossing occurred ~12 d_i downstream of an X line. Significant asymmetries in the plasma and field structures in the exhaust were observed in good agreement with PIC simulations.

2. Observations

On 31 October 2015 at 07:16–07:20 UT the four MMS spacecraft [*Burch et al.*, 2015] traversed the magnetopause at 13.4 magnetic local time on an outbound pass. The maximum interspacecraft separation was 12.7 km in X_{GSE}, 18.5 km in Y_{GSE}, and 14 km in Z_{GSE}. We use data from the magnetometer at 128 samples/s (Fluxgate Magnetometer) [*Russell et al.*, 2014], the fast plasma experiment (FPI) [*Pollock et al.*, 2016] at 30 ms resolution for electrons and 150 ms for ions, and the electric field instrument at 8192 samples/s [*Lindqvist et al.*, 2014; *Torbert et al.*, 2014].

Figures 1a–1k show MMS4 observations from 07:16:40 UT to 07:20:00 UT, in GSE coordinates. Initially, the spacecraft were located inside the magnetosphere, characterized by large T_i (>1 keV), low ion density (<2 cm^{-3}), and stable and northward B_z component (~40 nT). At 07:16:59 UT the spacecraft crossed the magnetopause and entered a region with higher density (~6–12 cm^{-3}), lower ion temperature (~400 eV), and intervals of plasma jetting with speed up to 160 km/s, indicative of magnetopause reconnection. Further evidence for reconnection is the presence of interpenetrating ion beams indicative of magnetic connection across the magnetopause (Figure 1l). At 07:18:38 UT a sharp reversal in the B_X component from ~ −12 nT to ~ +36 nT was observed. The B_X reversal coincided with a maximum in the magnetic field magnitude ($|B| = 57$ nT), a jet reversal mainly in V_Y (relative to the magnetosheath V_Y of 84 km/s), and a sharp discontinuity in V_Z. Previous studies of flux ropes with both field and flow reversals have been interpreted as the flux ropes being flanked by two active X lines [e.g., *Hasegawa et al.*, 2010; *Øieroset et al.*, 2011, 2014]. The presence of O^+ (Figure 1e) inside the flux rope indicates that the flux rope was connected to the magnetosphere. O^+ was not present in the magnetosheath proper (beyond the interval in Figure 1). The flux rope was unusual in that the magnetic shear across it was rather small (26°) due to the northward interplanetary magnetic field. The MMS flux rope crossing time was 90 s, from when B_X started to decrease from its magnetospheric value (at 07:17:41 UT) to when it changed to the magnetosheath value (at 07:19:11 UT; see vertical lines in Figure 1). This corresponds to a crossing distance of 8000 km based on the normal speed of 89 km/s of the thin current sheet at the flux rope center (see below), or 100 d_i (based on a density of 8 cm^{-3}).

A never before reported aspect of a flux rope is the presence of a plasma jet with a speed of >100 km/s (relative to the adjacent regions) in the negative X direction during the sharp B_X reversal at 07:18:38 UT (Figure 1g). The jet indicates that at the center of the flux rope the B_X reversal and converging flows formed a compressed current sheet which itself underwent reconnection. This thin reconnecting current sheet was characterized by clear electron heating with $\Delta T_{e\|} \sim 30$ eV (Figure 1i), a maximum in the current density up to ~0.4 μAm^{-2} (Figure 1j), and enhanced electric field magnitude up to ~27 mV/m (Figure 1k). The current sheet formed by the B_X reversal had approximately symmetric boundary conditions and a magnetic shear of 45°; i.e., the guide field was about two times the reconnecting magnetic field. The crossing duration of the thin current sheet was only 2 s. Thin current sheets at the center of active flux ropes have been observed previously [*Hasegawa et al.*, 2010; *Øieroset et al.*, 2011, 2014] but could not be resolved by plasma instruments on previous spacecraft missions.

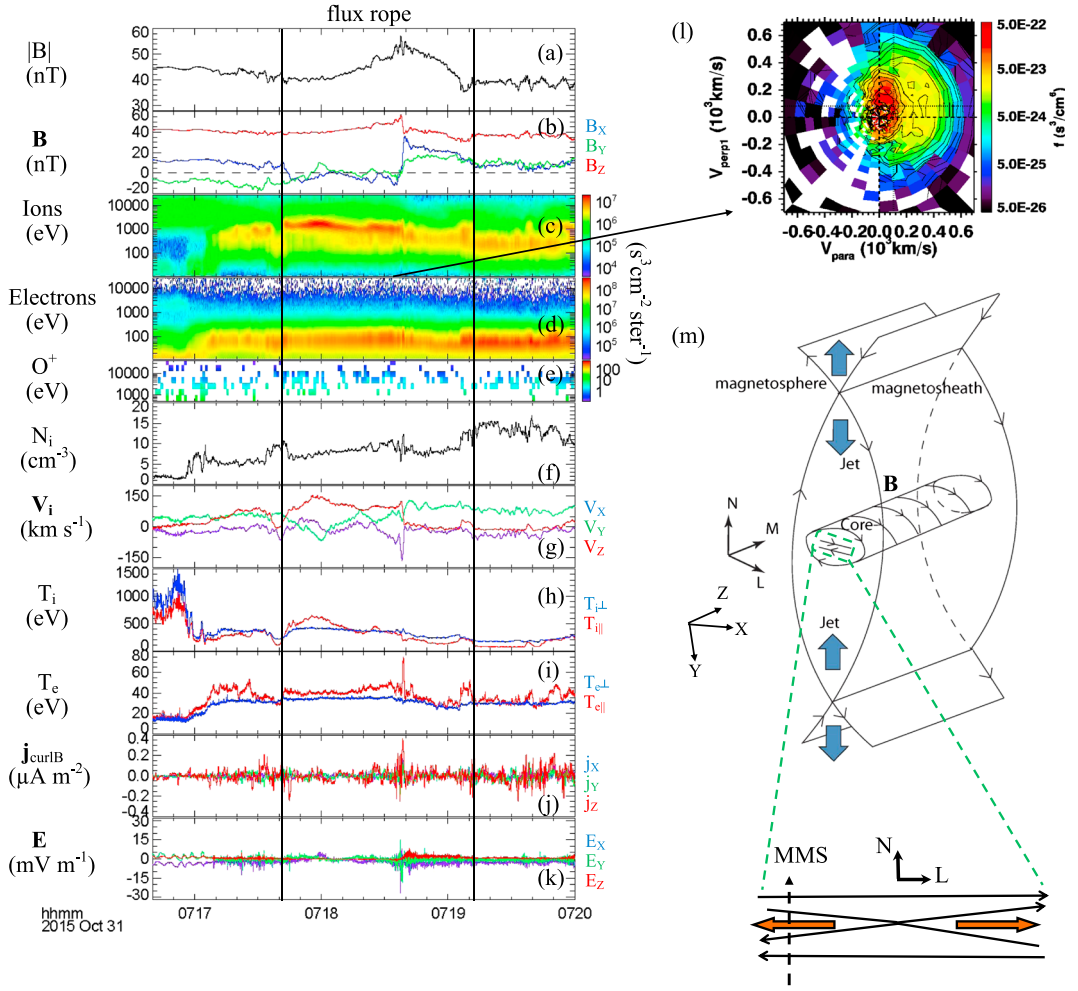

Figure 1. MMS4 flux rope observations in GSE coordinates. (a) Magnetic field magnitude, (b) magnetic field, (c) ion spectrogram in energy flux, (d) electron spectrogram in energy flux, (e) O^+ counts (eV), (f) ion density, (g) ion velocity, (h) ion temperature, (i) electron temperature, (j) current calculated using plasma data, (k) electric field, (l) 2-D cut of the 3-D ion distribution at 07:18:36.555–07:18:36.705 UT, and (m) simplified cartoon showing the location of the thin current sheet inside a flux rope. The vectors inside the green box represent the reconnecting component of the magnetic field. In the LMN coordinate system L = GSE(0.890, 0.309, −0.335), M = GSE(0.333, 0.0627, 0.941), and N = GSE(0.311, −0.949, −0.0470).

Figures 2a–2k show observations from all four MMS spacecraft, in and near the current sheet. The observations from each spacecraft are overlaid in each panel for comparison. The observations are now presented in the current sheet boundary normal (*LMN*) coordinate system obtained from the minimum variance analysis of the MMS4 magnetic field for the 07:18:36–07:18:41 UT interval. *L* is along the reconnecting magnetic field direction, *M* is along the X line, and *N* is along the thin current sheet normal (Figure 1m). The observations from each spacecraft were nearly identical, indicating that the observed structures were stable (at least during the spacecraft crossing time) and moved with a constant speed. Multispacecraft timing analysis [*Schwartz*, 1998; *Dunlop et al.*, 2002] indicates that the current sheet (and the flux rope) moved duskward and tailward in the current sheet normal direction (where $\boldsymbol{N}$ = GSE(−0.3035, 0.9527, 0.01376)) with a speed of 89 km/s, which is similar to the external magnetosheath flow speed and direction of $V_X = -40$ km/s and $V_Y = 84$ km/s. The normal from the multispacecraft timing analysis differs by only 2° from the normal calculated from minimum variance analysis. The constant velocity of the current sheet past the spacecraft means that the time series correspond approximately to spatial profiles.

The current density has been calculated using both the curlometer technique [*Robert et al.*, 1998] and the current measured by each MMS plasma instrument averaged at the barycenter of the spacecraft tetrahedron

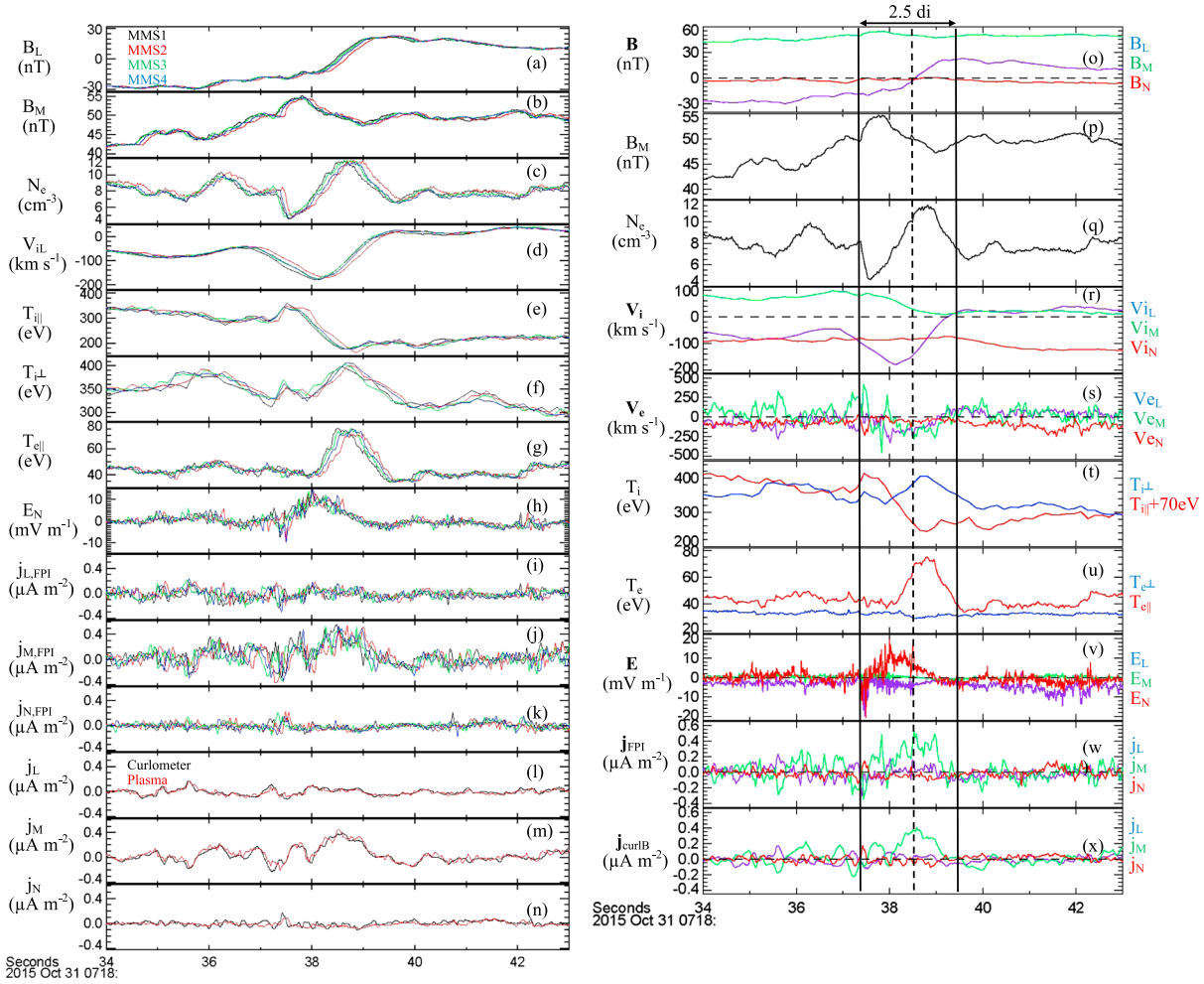

Figure 2. Multispacecraft MMS observations in and near the current sheet in *LMN* coordinates (black: MMS1, red: MMS2, green: MMS3, blue: MMS4): (a) reconnecting magnetic field, (b) out-of-plane magnetic field, (c) electron density, (d) ion outflow, (e) parallel ion temperature, (f) perpendicular ion temperature, (g) parallel electron temperature, (h) normal electric field, and (i–k) current along the *L*, *M*, and *N* directions calculated from the plasma measurements. (l–n) Current along *L*, *M*, and *N* calculated using observations from all four spacecraft. Black curve: using the curlometer technique on the magnetic field data, red curve: using the barycenter method on the plasma data. Detailed MMS4 observations: (o) magnetic field, (p) out-of-plane magnetic field, (q) electron density, (r) ion velocity, (s) electron velocity, (t) ion temperature, (u) electron temperature, (v) electric field, (w) current from plasma data, and (x) current from the curlometer technique on all four spacecraft.

(Figures 2l and 2m). The two independent methods show remarkable agreement, which suggests that the considerable variation in the current density across the exhaust is the result of a spatial structure convecting past the spacecraft.

Figures 2o–2x show the detailed MMS4 observations. The magnetic field rotation across the thin current sheet was 45°. The ~45 nT guide field (B_M just outside the current sheet) was about 2 times the reconnecting field B_L. The plasma density was ~8 cm^{-3} on both sides of the current sheet. The rather weak asymmetries in the plasma and magnetic fields between the two inflow regions mean that the reconnection configuration was nearly symmetric, making this an ideal event to study symmetric reconnection with a large guide field.

The reconnection exhaust was observed for 2.2 s and is marked between the two vertical solid lines in Figures 2o–2x. Note that there is some ambiguity in where the exhaust starts on the left side in the plot. In comparison with simulation (Figure 3m) the location where the density starts to drop marks approximately the left (first) separatrix. With the current sheet propagation speed of 89 km/s the current sheet width was 196 km (or 2.5 d_i based on a density of 8 cm^{-3}). Assuming a reconnection rate of 0.1 (which corresponds to an exhaust opening angle of 11°) the distance between the spacecraft exhaust crossing location and the X line is estimated to be ~12 d_i. Thus, the spacecraft was relatively close to the X line but not in the electron diffusion

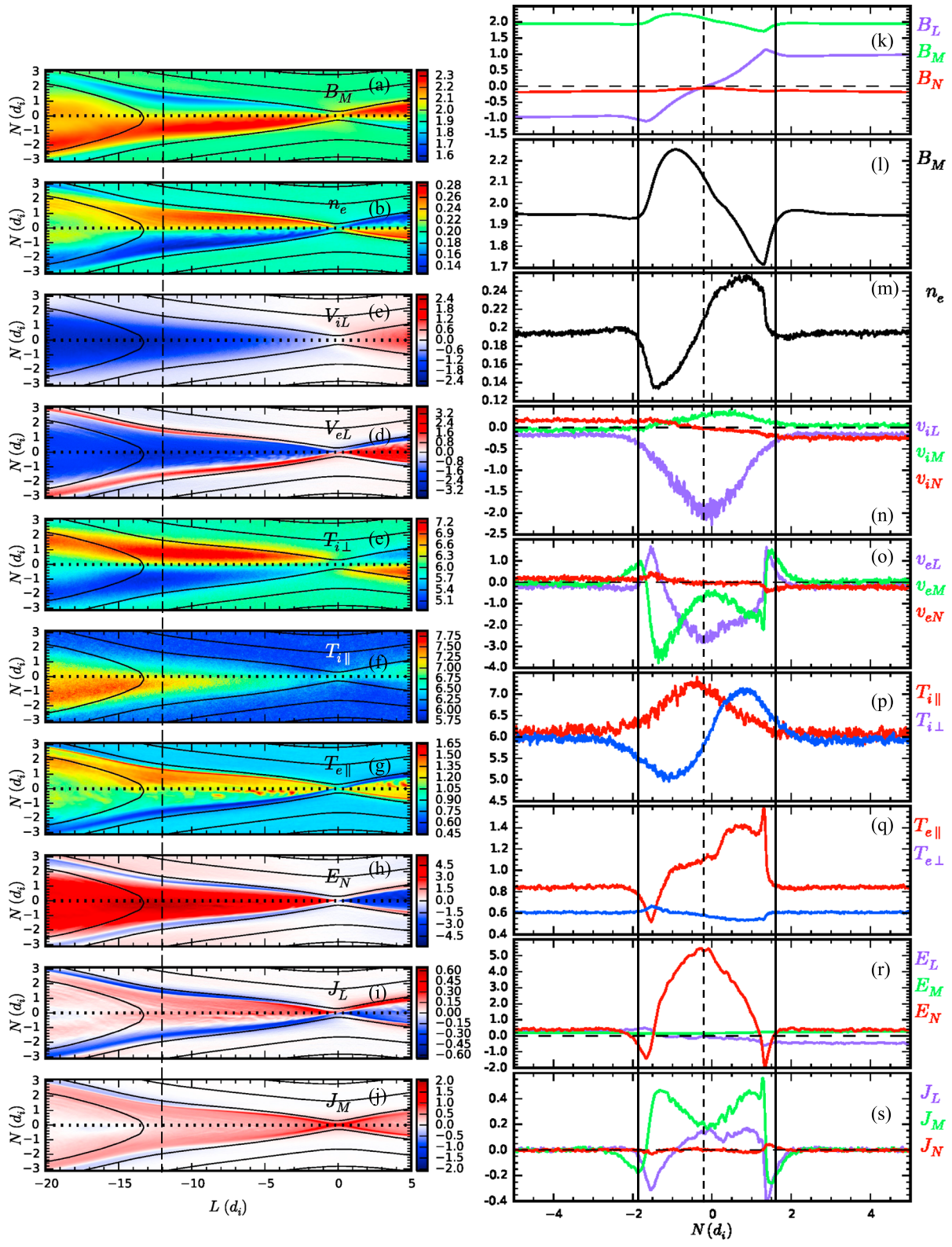

Figure 3. Results from 2D PIC simulations with *mi*/*me* = 100. The *LMN* coordinate system is the same as the one used in Figure 2. *N* is along the current sheet normal, *M* along the X line direction (positive into the plane), and *L* along the outflow direction. Lengths are plotted in units of the ion inertial length in the inflow region. Simulation results in the *N*-*L* plane: (a) the out-of-plane magnetic field, (b) electron density, (c) ion outflow, (d) electron outflow, (e) perpendicular ion temperature, (f) parallel ion temperature, (g) parallel electron temperature, (h) the Hall electric field, (i) the in-plane current, and (j) the out-of-plane current. (k–s) Plasma and field parameters from the simulation along a cut at $L = -12\ d_i$ (marked with the vertical dashed line in Figures 3a–3j). The order of the parameters corresponds to the observed parameters in Figure 2.

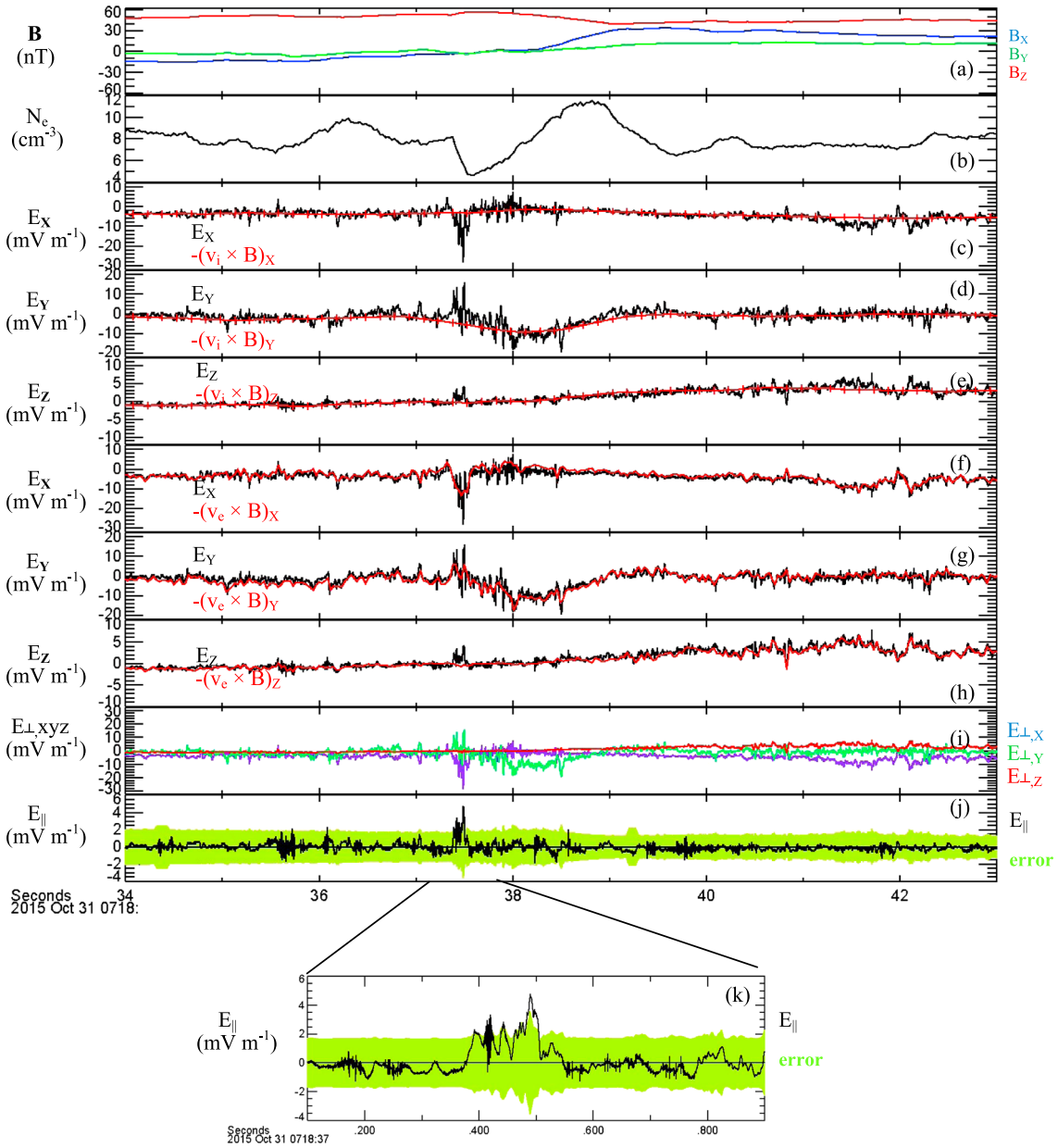

Figure 4. MMS4 electric field measurements and $-\mathbf{v_i}\times\mathbf{B}$ and $-\mathbf{v_e}\times\mathbf{B}$, in DSL (spacecraft) coordinates, which are nearly identical to GSE. (a) magnetic field, (b) electron density, (c) E_X and $-(\mathbf{v_i}\times\mathbf{B})_X$, (d) E_Y and $-(\mathbf{v_i}\times\mathbf{B})_Y$, (e) E_Z and $-(\mathbf{v_i}\times\mathbf{B})_Z$, (f) E_X and $-(\mathbf{v_e}\times\mathbf{B})_X$, (g) E_Y and $-(\mathbf{v_e}\times\mathbf{B})_Y$, (h) E_Z and $-(\mathbf{v_e}\times\mathbf{B})_Z$, (i) perpendicular electric field, (j) parallel electric field with error (in green), and (k) zoom-in of parallel electric field with error (in green).

region surrounding the X line. This is confirmed by the comparison between the observed electric field and $-\mathbf{v_i}\times\mathrm{B}$ and $-\mathbf{v_e}\times\mathrm{B}$ (Figure 4), which reveal that the ions were not frozen-in at the separatrices as well as in parts of the exhaust, while the electrons were frozen-in throughout the exhaust, except perhaps at the left separatrix. At the left separatrix, the measured perpendicular electric field was large (~25 mV/m), while there is an apparent positive parallel electric field up to 5 mV/m (Figure 5j). However, the uncertainty in the parallel electric field is of comparable magnitude. Thus, it is unclear how much of this field is real.

Inside the current sheet the observations show distinct asymmetries with respect to the midplane ($B_L = 0$) in the out of plane magnetic field component (Figure 2p), electron density (Figure 2q), ion temperature (Figure 2t), and electron temperature (Figure 2u). To the left of the midplane (marked by the vertical dashed line) the plasma density displays a density dip and to the right a density enhancement. These density "perturbations"

covered the entire exhaust and were not restricted to the separatrices. The perpendicular and parallel ion temperatures were enhanced on opposite sides of the exhaust midplane, with $T_{i||}$ enhanced on the low-density side and $T_{i\perp}$ enhanced on the high-density side. Furthermore, the parallel electron temperature was strongly enhanced (from ~45 eV to 75 eV) on the high density side, while $T_{e\perp}$ displayed no heating or perhaps even slight cooling (from ~34 to ~30 eV) at the location where $T_{e||}$ was enhanced.

The normal component of the electric field was mostly positive inside the exhaust, where it reached 20 mV/m (Figure 2v). Near the left edge of the exhaust E_N showed a large negative dip. There might also be a much smaller dip in E_N at the right (second) edge. The out-of-plane magnetic field B_M displayed a positive perturbation followed by a negative perturbation during the current sheet crossing (Figure 2p).

The current densities calculated from the single-spacecraft FPI plasma data using $\mathbf{j} = ne(\mathbf{v_i} - \mathbf{v_e})$, where n is the plasma density, e is the elementary coulomb charge, and $\mathbf{v_i}$ and $\mathbf{v_e}$ are the ion and electron velocities, and from the curlometer technique [*Dunlop et al*., 2002] show good overall agreement. Two peaks in the out-of-plane current density up to ~0.4–0.6 μAm^{-2} were seen during the exhaust crossing (Figures 2w and 2x).

3. Comparison With Simulations

Figure 3 shows results from a 2.5-D collisionless reconnection simulation generated with the particle-in-cell (PIC) code P3D [*Zeiler et al*., 2002]. Magnetic field strengths and number densities are normalized to arbitrary simulation units B_0 and n_0, respectively. Lengths are then normalized to the ion skin depth $d_{i0} = c/\omega_{pi0}$ at the reference density n_0, and times are normalized to the ion cyclotron time $(\Omega_{ci0})^{-1} = m_i c/eB_0$. Velocities are normalized to the Alfvén speed $c_{A0} = B_0/\sqrt{(4\pi m_i n_0)} = d_{i0}/(\Omega_{ci0})^{-1}$, electric fields to $E_0 = c_{A0}B_0/c$ and temperatures to $T_0 = m_i {c_{A0}}^2$. An artificial ion to electron mass ratio and speed of light were set to $m_i/m_e = 100$ and $c/c_{A0} = 30$, respectively. The simulation domain is $L_x \times L_y = 204.8 \times 102.4\ d_{i0}$, with grid spacing $\Delta x = 0.025$, time step $\Delta t = 0.0025$, and periodic boundary conditions. The simulation was initialized with a double current sheet [*Shay et al*., 2007], with an out of plane (guide) magnetic field twice the reconnecting field $B_M = 2B_L = 2.0B_0$, an upstream density of $n_0 = 0.2$ and with electron and ion temperatures of .618 T_0 and 6.18 T_0 to match the observed plasma beta and temperature ratio of the observation. The simulation was evolved until it reached a steady state, and then was averaged over 100 time steps to smooth the data. The data were rotated into the same *LMN* coordinate system for direct comparison with observations, and the lengths in Figure 3 are renormalized to the upstream ion skin depth using the inflowing density $n = 0.2$.

The large guide field gives rise to asymmetries across the reconnection exhausts. The out of plane quadrupolar Hall magnetic field (Figure 3a) is skewed and extends across the midplane on the side where it points in the same direction as the guide field. A skewed Hall magnetic field was also reported by *Eastwood et al*. [2010b], although that event had a much weaker guide field. The plasma density (Figure 3b) is reduced on one side of the exhaust midplane and enhanced on the other side. The perpendicular and parallel ion temperatures are enhanced on opposite sides of the exhaust midplane. The parallel electron temperature is enhanced on the same side as the perpendicular ion temperature (which is also the side where the density is enhanced). The normal electric field fills most of the exhaust and is positive on the left side of the X line (Figure 3h). The out-of-plane current is strongest at the X line but remains large in the exhaust where it splits into two branches downstream away from the X line, leaving a minimum near the exhaust midplane (Figure 3j).

We now compare the observations (Figure 2) with the predictions from the simulation. We estimated that the observed exhaust was 2.5 d_i wide and that MMS crossed the exhaust ~12 d_i downstream of an X line. Figures 3k–3s show parameters from the simulation along a cut at $L = -12\ d_i$, where the exhaust width is about 3.5 d_i. This suggests that the exhaust crossing by MMS may be even closer than 12 d_i away from the X line. Nevertheless, many of the plasma and field profiles are well reproduced. The simulated Hall magnetic and electric field spatial profiles are similar to the observed profiles. Furthermore, the qualitative agreement between the observed and predicted asymmetries in the ion and electron perpendicular and parallel temperatures as well as in the plasma density is remarkable. However, there are also some differences. The predicted profile of the out of plane current (Figure 3s, green curve) exhibits two peaks, similar to the observations (Figures 2w and 2x). However, one of the peaks in the observations extends past the midplane, whereas the simulated current is more symmetric about the midplane. Furthermore, the j_L profile (Figure 3s, blue curve) in the simulation shows two distinct dips at the edges of the exhaust, which are not discernable in

the observations (Figures 2w and 2x, blue curves). Overall, however, the qualitative agreement between observations and simulation is considered excellent.

4. Discussion and Summary

While the focus of this study is on the ion-scale current sheet formed at the center of a magnetic flux rope, the observation of reconnection inside a flux rope is in itself interesting. There are at least two scenarios that could give rise to reconnection inside a flux rope. First, larger flux ropes (or islands) are often thought to be formed by coalescence of smaller flux ropes (or islands). Such a scenario is commonly seen in simulations [e.g., *Oka et al*., 2010] but has rarely been observed in space, although its consequences have been reported [*Retinò et al*., 2008; *Wang et al*., 2015]. Direct evidence of coalescence would be the detection of reconnection jets at the center of a large flux rope, similar to what is observed in this event. However, we do not see evidence for the two smaller flux ropes that are undergoing coalescence since the normal magnetic field (B_X in Figure 1) only showed a single bipolar variation rather than a pair of bipolar variation as expected for two flux ropes. It is unclear whether or not the absence of the latter is due to the slanted nature of the spacecraft trajectory through the flux rope.

An alternative (and very different) scenario (depicted in Figure 1m) is that the current sheet at the flux rope center was formed between field lines carried by the converging jets from the two X lines forming the flux rope. In this scenario reconnection happens when the reconnected field lines meet at the center of the flux rope. How this reconnection happens is still an intriguing question since it implies that oppositely directed field lines carried by the converging jets reconnect as the jets collide. This collision is unlikely to happen in 2-D systems because the restoring magnetic tension force would prevent the oppositely directed magnetic field lines from meeting at the center of an island. Indeed, such a scenario has not been reported in 2-D simulations of multiple X line reconnection. However, in 3-D the scenario could be plausible since the field lines do not form closed loops.

Regardless of the scenario that created the thin current sheet in this event, the nearly symmetric and strong guide field configuration, together with the constant propagation speed of the current sheet, allowed the study of the exhaust structure of a rarely observed reconnection regime in the magnetophere. This MMS event, together with the simulation, shows that strong guide field symmetric reconnection is characterized by a shift in the ion and electron temperature anisotropy across the reconnection exhaust, with $T_{i||}$ and $T_{i\perp}$ being enhanced on opposite sides of the exhaust midplane and $T_{e||}$ being enhanced on the side where $T_{i\perp}$ is enhanced. A large asymmetry is also seen in the plasma density across the exhaust, with a density minimum on the side where $T_{i||}$ is enhanced, and a density maximum on the side where $T_{i\perp}$ and $T_{e||}$ are enhanced.

The large guide field is the key to understanding the observed asymmetries across the exhaust. In guide field reconnection, density cavities form along two of the four separatrices [*Pritchett and Coroniti*, 2004]. Parallel electric fields along the low-density separatrix accelerate electrons toward the X line and eject them out along the opposite (high-density) side of the exhaust. The high-density side of the exhaust is made up of the mixing of the accelerated electrons and the inflowing electrons, which leads to an enhanced electron temperature, while the density cavities have lower temperature [*Drake et al*., 2005]. This predicted correlation between electron temperature and density in the exhaust was seen in the MMS observations (Figures 2q and 2u). While the observed parallel electric field on the low-density side is consistent with the scenario described above, the experimental evidence for the parallel electric field is marginal due to the large uncertainty in the measurements. Note that parallel electric fields along the separatrix have also been reported in symmetric reconnection observations in the magnetotail under smaller guide field conditions [e.g., *Wang et al*., 2013] as well as for asymmetric reconnection at the magnetopause [*Mozer and Pritchett*, 2010].

For the asymmetries seen in the ion parameters, the key is again the guide field. The large guide field, coupled with the outflow, leads to a normal electric field that span across the exhaust. Ions that cross the separatrix into the exhaust move in the direction of the normal electric field in cusp-like orbits [*Drake et al*., 2009]. The result is that the perpendicular temperature and density are larger on the side of the exhaust where the ions turn around, i.e., on the side of the exhaust where E_N points toward the inflow. The cause of the ion parallel temperature shift, although also seen in the simulations (Figure 3p) [see also *Drake and Swisdak*, 2014], is currently not understood.

The event presented here constitutes the first direct observation of magnetic reconnection between colliding jets in a compressed thin current sheet at the center of a magnetic flux rope. Such a scenario may not be rare, and their impact on flux rope dynamics should be explored in future studies.

Acknowledgments
This research was supported by STFC (UK) grants ST/K001051/1 and ST/N000692/1 and NSF grant AGS-1103303 and NASA grants NNX13AD72G and NNX08AO83G at UC Berkeley and NASA grant NNX15AW58G at U Delaware. Simulations and analysis were performed at the National Center for Atmospheric Research Computational and Information System Laboratory (NCAR-CISL) and at the National Energy Research Scientific Computing Center (NERSC). IRAP contribution to MMS was supported by CNES and CNRS. Data source: MMS Science Data Center at lasp.colorado.edu/mms/sdc/public/

References

Burch, J. L., T. E. Moore, R. B. Torbert, and B. L. Giles (2015), Magnetospheric Multiscale overview and science objectives, *Space Sci. Rev.*, 1–17, doi:10.1007/s11214-015-0164-9.

Drake, J. F., and M. Swisdak (2014), The onset of ion heating during magnetic reconnection with a strong guide field, *Phys. Plasmas*, *21*, 072903, doi:10.1063/1.4889671.

Drake, J. F., M. A. Shay, W. Thongthai, and M. Swisdak (2005), Production of energetic electrons during magnetic reconnection, *Phys. Rev. Lett.*, *94*, 095001, doi:10.1103/PhysRevLett.94.095001.

Drake, J. F., P. A. Cassak, M. A. Shay, M. Swisdak, and E. Quataert (2009), A magnetic reconnection mechanism for ion acceleration and abundance enhancements in impulsive flares, *Astrophys. J.*, *700*, L16–L20, doi:10.1088/0004-637X/700/1/L16.

Dunlop, M. W., A. Balogh, K.-H. Glassmeier, and P. Robert (2002), Four-point Cluster application of magnetic field analysis tools: The Curlometer, *J. Geophys. Res.*, *107*(A11), 1384, doi:10.1029/2001JA0050088.

Eastwood, J. P., T. D. Phan, M. Øieroset, and M. A. Shay (2010a), Average properties of the magnetic reconnection ion diffusion region in the Earth's magnetotail: The 2001–2005 Cluster observations and comparison with simulations, *J. Geophys. Res.*, *115*, A08215, doi:10.1029/2009JA014962.

Eastwood, J. P., M. A. Shay, T. D. Phan, and M. Øieroset (2010b), Asymmetry of the ion diffusion region hall electric and magnetic fields during guide field reconnection: Observations and comparison with simulations, *Phys. Rev. Lett.*, *104*, 205001.

Gosling, J. T., and A. Szabo (2008), Bifurcated current sheets produced by magnetic reconnection in the solar wind, *J. Geophys. Res.*, *113*, A10103, doi:10.1029/2008JA013473.

Gosling, J. T., and T. D. Phan (2013), Magnetic reconnection in the solar wind at current sheets associated with extremely small field shear angles, *Astrophys. J.*, *763*, L39.

Gosling, J. T., R. M. Skoug, D. J. McComas, and C. W. Smith (2005), Direct evidence for magnetic reconnection in the solar wind near 1 AU, *J. Geophys. Res.*, *110*, A01107, doi:10.1029/2004JA010809.

Hasegawa, H., J. Wang, M. W. Dunlop, Z. Y. Pu, Q. H. Zhang, B. Lavraud, and M. G. G. T. Taylor (2010), Evidence for a flux transfer event generated by multiple X-line reconnection at the magnetopause, *Geophys. Res. Lett.*, *37*, L16101, doi:10.1029/12010GL044219.

Lindqvist, P.-A., et al. (2014), The spin-plane double probe electric field instrument for MMS, *Space Sci. Rev.*, 1–29, doi:10.1007/s11214-014-0116-9.

Mozer, F. S., and P. L. Pritchett (2010), Spatial, temporal, and amplitude characteristics of parallel electric fields associated with subsolar magnetic field reconnection, *J. Geophys. Res.*, *115*, A04220, doi:10.1029/2009JA014718.

Øieroset, M., et al. (2011), Direct evidence for a three-dimensional magnetic flux rope flanked by two active magnetic reconnection X lines at Earth's magnetopause, *Phys. Rev. Lett.*, *107*, 165007.

Øieroset, M., D. Sundkvist, C. C. Chaston, T. D. Phan, F. S. Mozer, J. P. McFadden, V. Angelopoulos, L. Andersson, and J. P. Eastwood (2014), Observations of plasma waves in the colliding jet region of amagnetic flux rope flanked by two active X lines at the subsolar magnetopause, *J. Geophys. Res. Space Physics*, *119*, 6256–6272, doi:10.1002/2014JA020124.

Oka, M., T.-D. Phan, S. Krucker, M. Fujimoto, and I. Shinohara (2010), Electron acceleration by multi-island coalescence, *Astrophys. J.*, *714*, 915.

Phan, T. D., J. F. Drake, M. A. Shay, F. S. Mozer, and J. P. Eastwood (2007a), Evidence for an elongated (>60 ion skin depths) electron diffusion region during fast magnetic reconnection, *Phys. Rev. Lett.*, *99*, 255002.

Phan, T. D., G. Paschmann, C. Twitty, F. S. Mozer, J. T. Gosling, J. P. Eastwood, M. Øieroset, H. Rème, and E. A. Lucek (2007b), Evidence for magnetic reconnection initiated in the magnetosheath, *Geophys. Res. Lett.*, *34*, L14104, doi:10.1029/2007GL030343.

Phan, T. D., J. T. Gosling, G. Paschmann, C. Pasma, J. F. Drake, M. Øieroset, D. Larson, R. P. Lin, and M. S. Davis (2010), The dependence of magnetic reconnection on plasma β and magnetic shear: Evidence from solar wind observations, *Astrophys. J.*, *719*, L199.

Phan, T. D., T. E. Love, J. T. Gosling, G. Paschmann, J. P. Eastwood, M. Øieroset, V. Angelopoulos, J. P. McFadden, D. Larson, and U. Auster (2011), Triggering of magnetic reconnection in a magnetosheath current sheet due to compression against the magnetopause, *Geophys. Res. Lett.*, *38*, L17101, doi:10.1029/2011GL048586.

Pollock, C., et al. (2016), Fast plasma investigation for magnetospheric multiscale, *Space Sci. Rev.*, doi:10.1007/s11214-016-0245-4.

Pritchett, P. L., and F. V. Coroniti (2004), Three-dimensional collisionless magnetic reconnection in the presence of a guide field, *J. Geophys. Res.*, *109*, A01220, doi:10.1029/2003JA009999.

Retino, A., D. Sundkvist, A. Vaivads, F. Mozer, M. André, and C. J. Owen (2007), In situ evidence of magnetic reconnection in turbulent plasma, *Nat. Phys.*, *3*, 235–238, doi:10.1038/nphys574.

Retinò, A., et al. (2008), Cluster observations of energetic electrons and electromagnetic fields within a reconnecting thin current sheet in the Earth's magnetotail, *J. Geophys. Res.*, *113*, A12215, doi:10.1029/2008JA013511.

Robert, P., M. W. Dunlop, A. Roux, and G. Chanteur (1998), Accuracy of current density determination, in *Analysis Methods for Multi-Spacecraft Data*, edited by G. Paschmann and P. W. Daly, pp. 395–418, Intl. Space Sci. Inst., Bern.

Russell, C. T., et al. (2014), The Magnetospheric Multiscale magnetometers, *Space Sci. Rev.*, 1–68, doi:10.1007/s11214-014-0057-3.

Schwartz, S. J. (1998), Shock and discontinuity normals, Mach numbers and related parameters, in *Analysis Methods for Multi-spacecraft Data*, edited by G. Paschmann and P. W. Daly, pp. 249–270, Intl. Space Sci. Inst., Bern.

Shay, M. A., J. F. Drake, and M. Swisdak (2007), Two-scale structure of the electron dissipation region during collisionless magnetic reconnection, *Phys. Rev. Lett.*, *99*, 155002.

Torbert, R. B., et al. (2014), The FIELDS instrument suite on MMS: Scientific objectives, measurements, and data products, *Space Sci. Rev.*, doi:10.1007/s11214-014-0109-8.

Wang, R., R. Nakamura, Q. Lu, A. Du, T. Zhang, W. Baumjohann, and Y. V. Khotyaintsev (2012), Asymmetry in the current sheet and secondary magnetic flux ropes during guide field magnetic reconnection, *J. Geophys. Res.*, *117*, A07223, doi:10.1029/2011JA017384.

Wang, R., A. Du, R. Nakamura, Q. Lu, Y. V. Khotyaintsev, M. Volwerk, T. Zhang, E. A. Kronberg, P. W. Daly, and A. N. Fazakerley (2013), Observation of multiple sub-cavities adjacent to single separatrix, *Geophys. Res. Lett.*, *40*, 2511–2517, doi:10.1002/grl.50537.

Wang, R., Q. Lu, R. Nakamura, C. Huang, A. Du, F. Guo, W. Teh, M. Wu, S. Lu, and S. Wang (2015), Coalescence of magnetic flux ropes in the ion diffusion region of magnetic reconnection, *Nat. Phys.*, *12*, doi:10.1038/NPHYS3578.

Zeiler, A., D. Biskamp, J. F. Drake, B. N. Rogers, and M. A. Shay (2002), Three dimensional particle simulations of collisionless magnetic reconnection, *J. Geophys. Res.*,*107*(A9), 1230, doi:10.1029/2001JA000287.